2015-02-02

Integration of Antenna Array with Multicrystalline Silicon Solar Cell

Oisin O'Conchubhair
Technological University Dublin, oisin.oconchubhair@mydit.ie

Patrick McEvoy
Technological University Dublin, patrick.mcevoy@tudublin.ie

Max Ammann
Technological University Dublin, max.ammann@tudublin.ie

Recommended Citation

O'Conchubhair, O.; McEvoy, P.; Ammann, M.J., "Integration of Antenna Array With Multicrystalline Silicon Solar Cell," *Antennas and Wireless Propagation Letters, IEEE* , vol.14, pp.1231,1234, 2015 doi:10.1109/LAWP.2015.2399652

Integration of Antenna Array with Multicrystalline Silicon Solar Cell

Oisin O'Conchubhair, Patrick McEvoy, *Senior Member, IEEE,*
and Max J. Ammann, *Senior Member, IEEE*

***Abstract*— The integration of a low-profile antenna array with a multicrystalline silicon solar cell capable of powering a low power wireless sensor at 2.45 GHz is reported. Lattice bus bars on the cell are exploited to minimize antenna shadows from low profile antennas and transmission lines for a higher output power. The dual inverted-F array improves gain and beam switching enables the array to sweep a wider coverage angle with larger beamwidths compared to other solar integrated antennas.**

***Index Terms*— Antenna Array, Low Profile Printed Inverted-F Antenna, Solar Integration, Multicrystalline Solar Cell.**

I. Introduction

REMOTE monitoring of environmental conditions for control of temperature and humidity in horticultural growing houses is one of the emerging applications where autonomous sensors are linked with radio networks. Industrial glasshouses can be 8 m high with an area of 0.90 km^2 and battery maintenance of portable units can become a considerable expense. Solar cells are an alternate power source and can be integrated with the antenna to minimize the unit volume and to enable portable deployment. Both amorphous (a-Si) and crystalline (c-Si) type silicon solar cells with integrated antennas were reported but designs that minimize antenna footprints and related solar shadowing remain a challenge.

A-Si cells are lower cost, flexible and easily trimmed to fit a desired shape. Outputs of 3 V (~ 66 mW) or greater simplifies design of the associated circuitry but solar efficiencies are typically limited to ~10%. The co-siting of a 920 MHz coplanar waveguide inverted-F antenna (IFA) with a-Si solar cells [1] demonstrated the isolation of the antenna and solar functions to avoid mutual interference. The antenna occupied 25% of the available solar footprint. In [2], an enhanced integration approach configured a-Si cells with an aperture-coupled 2.4 / 5.2 GHz slot antenna. However, the antenna occupied ~10% of the available footprint reducing the solar collecting area.

Manuscript received July 29, 2014. ; revised November 08, 2014; accepted January 31, 2015. Date of publication MMM DD, YYYY; date of current version MMM DD, YYYY. This work was part funded by the Irish Higher Education Authority under PRTLI Cycle 5 as part of the Telecommunication Graduate Initiative. O. O'Conchubhair, P. McEvoy and M. J. Ammann are with the Antenna & High Frequency Research Centre, School of Electrical and Electronic Engineering, Dublin Institute of Technology, Kevin St., Dublin 8, Ireland (e-mail: oisin.oconchubhair@mydit.ie; patrick.mcevoy@dit.ie; max.ammann@dit.ie).

Alternatively, *mono-* and *multi*-crystalline silicon cells attain solar efficiencies up to 20% since crystalline structures have fewer electrical defects compared to a-Si. Their 0.5 V output (3.5 W) can necessitate the linking of a series of cells to obtain a useful circuit voltage. To avoid additional footprint extensions, it becomes preferable to vertically integrate the antenna while minimizing any solar shadowing. A panel of cells was configured above an antenna [3] which radiated through slot apertures that reduced the solar area by 6.5%.

An improved approach to overcome solar area loss due to apertures and shadowing is introduced in [4] where four cells within a monocrystalline solar panel are excited by a microstrip feed placed below the cell surface. The four cells also function as a 1.5 GHz patch antenna with a 12 mm total integrated height. Alternatively, a solution with an 8 mm height used a polycrystalline cell as a parasitic element above a planar IFA [5]. This ensured irradiation of the entire surface of the solar cell.

A solution with a 2 mm integrated height used a patch antenna over a polycrystalline cell [6]. However, the antenna plus the transmission line area shadow is a significant 13% of the solar cell area and additional cells are needed for suitable output voltages.

A solar concentrator was used as a parabolic reflector to enhance antenna gain and solar output by focusing the light on four emitter-wrap-through cells connected in-series to create a 1.5 GHz dipole antenna [7]. While the 2.2 V (73.8 mW) output could support a low powered sensor, the design is comparatively large for its output power. Another technique reports a parabolic reflector that is laminated with an unspecified cell type for a 12 GHz horn antenna [8].

To quantify the impact of a periodic lattice without a silicon sub-layer, the authors studied how a CPW-fed IFA coupled with a metallic lattice on FR-4 substrate [9]. The 1 dB drop in gain and 0.5% increase of bandwidth were partially due to a lack of isolation between the transmission feed and the lattice.

This paper introduces the integration of a two element array of low-profile IFAs with an alternative feed onto a full-sized 156 × 156 mm multicrystalline solar cell. The Solland cells have a rated output power of over 3 W for 1,000 W/m^2 test conditions with 0.45 W expected for annual average insolation levels of 150 W/m^2 in Northwest Europe [10]. This can power a wireless humidity sensor that demands less than 0.014 W per hour. The cell is capable of powering the sensor and charging a battery even in low light conditions if a high efficiency low

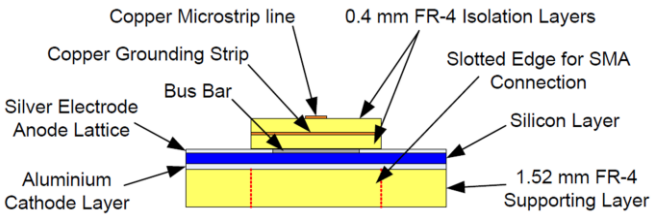

Fig. 1. Transmission line configuration

voltage boost converter like a Texas Instrument TPS61200 is used.

A 6 mm wide grounding strip between the transmission line and the cell adequately isolates the transmission line from the cell lattice, thereby improving gain, efficiency and bandwidth. Each antenna has a height of 6.9 mm above the cell and along with the transmission lines; the two antennas have a combined footprint which covers 5.30% of the solar cell surface.

II. Proposed Antenna Configurations

Fig. 1 shows a representative cross-section of the transmission line integrated with the Solland cell which consists of a 57-electrode silver anode front contact, a multicrystalline silicon inner layer and an aluminum cathode rear contact. The electrodes are 0.1 mm wide with two perpendicularly oriented 2 mm wide interconnecting bus bars with 74.18 mm edge separation for maximum power output. The solar cell sits on a 1.52 mm thick FR-4 substrate with slotted edges to accommodate soldering of SMA connectors to the transmission lines. The entire solar cell was simulated using CST Microwave Studio with a permittivity $\varepsilon_r = 20$ and a conductivity $\sigma = 242{,}270$ S/m for exposed multicrystalline silicon [6].

The 50 Ω microstrip lines (0.784 mm wide) are made with 0.4 mm thick FR-4 substrate over a 6 mm wide ground plane. The ground plane is isolated from the anode front contact by another 0.4 mm FR-4 layer.

The aluminum cathode layer is used as a ground plane for the array, with each transmission line positioned above one of the anode bus bars. The IFA employs 1 mm wide copper strip

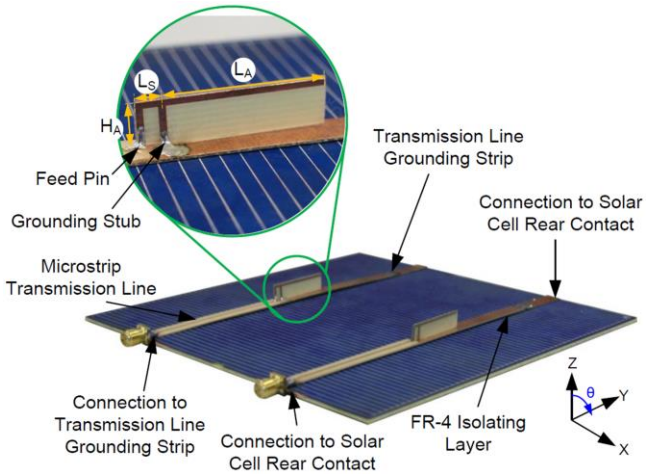

Fig. 2. Dual antenna configuration

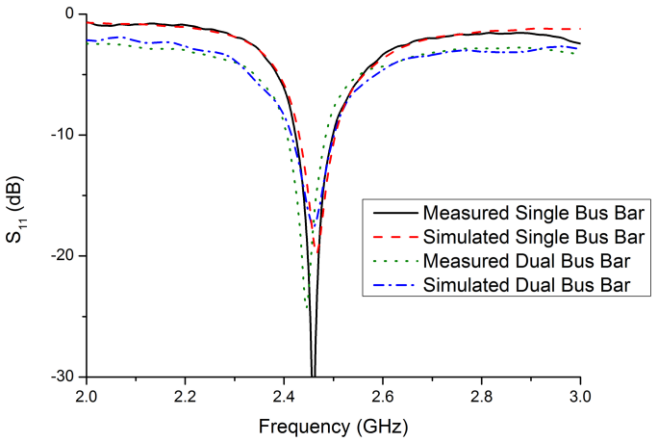

Fig. 3. Measured and simulated antenna S_{11} results

TABLE I
Single and Dual Antenna Results

Configuration & Analysis	Frequency (GHz)	-10 dB Bandwidth (%)	Boresight Gain (dBi)
Single Antenna Simulated	2.466	2.96	1.2
Single Antenna Measured	2.459	3.09	0.6
Dual Antenna Simulated	2.458	3.48	3.5
Dual Antenna Measured	2.446	3.22	3.5

on 0.4 mm FR-4 with $H_A = 6$ mm, $L_S = 3.5$ mm and $L_A = 22$ mm as shown in Fig. 2. In contrast to classical IFAs, the feed and shorting strips are reversed to facilitate improved grounding of the antenna (see inset Fig. 2). The anode lattice has inherent shadowing so the antennas are positioned over the bus-bars to minimize solar shadow on the cell.

The dual antenna array configuration is shown in Fig. 2. A non-integrated feed comprises a microstrip power splitter with quarter wave transformers to match to 50 Ω and with a 3.74 dB insertion loss at the resonant frequency.

III. Results and Discussion

The simulated and measured results for configuration; (a) single antenna located on one bus-bar; and (b) single antenna on each bus-bar (dual antenna) are given in Table I. S_{11} measurements and simulations are shown in Fig 3.

For an antenna and feed line positioned above one of the bus-bars, the area of exposed silicon is reduced by 2.65%. The measured boresight gain was 0.6 dBi with a bandwidth of 3.09% as shown in Fig. 4. However, the pattern becomes asymmetrical due to the off-center position of the antenna/bus-bar with respect to the ground plane. Both the single and dual antenna peak gains are in the Y-Z plane. While the configuration minimizes impact to the solar power output, the alteration of the radiation pattern is undesirable.

To improve the radiation symmetry and gain, an array was configured using an antenna spaced 76.18 mm apart on each bus-bar. While there is a cost in terms of a 5.30% solar shadow of the cell area, it is considerably less than previous patch antenna designs which covered 13%. If the antennas

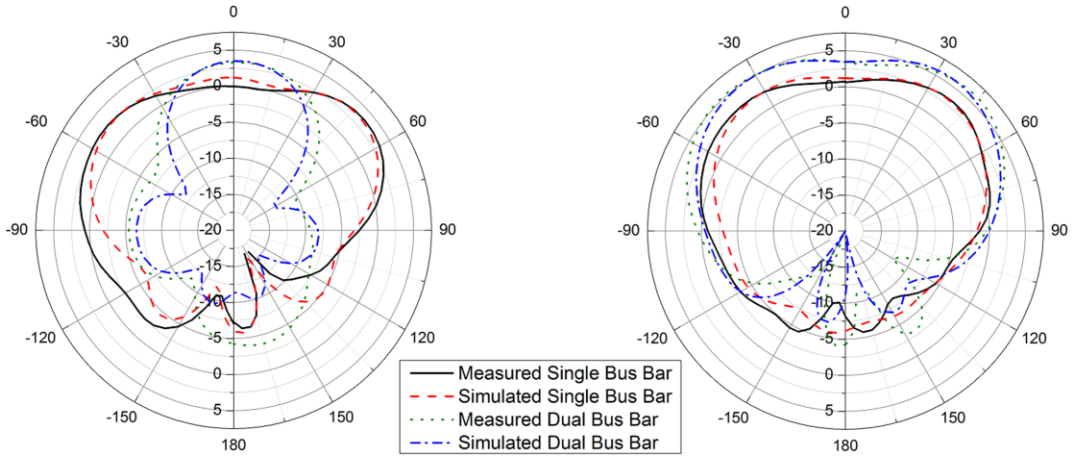

Fig. 4. Simulated and measured radiation pattern for X-Z plane (left) and Y-Z plane (right)

were moved off the bus bars and closer to each other, there would be a solar shadow of 7.89%. Fig. 5 shows that there is greater than 20 dB isolation between the two antennas. The measured bandwidth for the antenna array was 3.35%. The measured radiation pattern is more focused with 3.5 dBi boresight gain and 3-dB beamwidths of 60.2º and 144.8º for X-Z and Y-Z planes respectively. The simulated efficiency was 70.15%. This is a 1.8 dB gain improvement over a single antenna centrally-positioned on the solar cell (off bus-bar) and is more suited to applications that require greater range. Antenna position results are shown in Table II.

IV. Solar Shadowing

A 1450 Lux tungsten halogen directed light source was used to evaluate antenna shadowing on the cell. The light source is positioned 960 mm from a pivoting table used for angle of incidence measurements on solar cells. Shade due to the covered area is added to when the angles of incident light tend towards the plane of the solar cell. Extra shadows are projected from the vertical surfaces on the antenna and microstrip line profile.

Antenna shadows from the Y-Z plane remain over the 6 mm wide ground plane of the microstrip line but they extend beyond its surface when the angle of incidence $\theta \geq 24º$ for the X-Z plane. The shadow cast by the antenna and its transmission line minus the lattice as a result of the angle of the incidence was measured. For $\theta = 0º$, 5.30% shadowing of the solar cell area occurs. For $\theta = 30º$ it increases to 6.18% and for $\theta = 60º$, shadowing accounts for 9.65% coverage.

The effect of shadowing on the solar cell output was assessed by measuring the open-circuit voltage (V_{oc}) and short-circuit current (I_{sc}) for each of the sampled incident angles, shown in Table III.

The V_{oc} increases suggest that the addition of the antenna and the oblique incident angles allow the solar cell to cool slightly, thereby increasing the solar efficiency. I_{sc} decreases as the shadowing increases. Measured I-V Curves for each incident angle are shown in Fig. 6.

TABLE II
Measured Antenna Position Results

Antenna Configuration	Peak Realized Gain (dBi)	Beamwidth (º)	
		X-Z Plane	Y-Z Plane
Single Antenna off Bus-Bar	4.3	152.4	141.0
Single Antenna on Bus-Bar	3.8	166.5	199.7
Dual Antenna on Bus-Bars	6.5	60.2	144.8

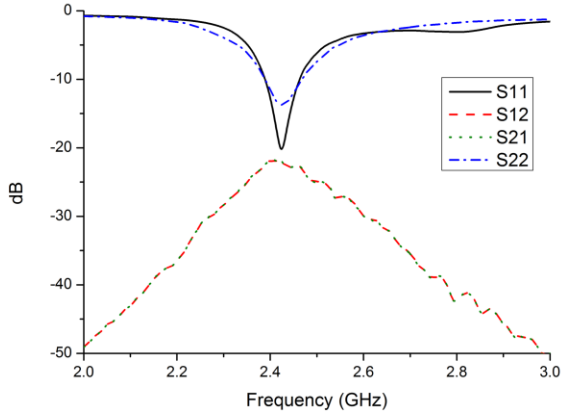

Fig. 5. Measured antenna coupling

TABLE III
V_{oc} and I_{sc} Results

Incident Angle	Shade (%)	V_{oc} (V)	I_{sc} (A)
No Antenna 0º	0	0.499	4.03
No Antenna 30º	0	0.513	3.01
No Antenna 60º	0	0.518	1.30
Dual Antenna 0º	5.30	0.506	3.81
Dual Antenna 30º	6.18	0.511	2.88
Dual Antenna 60º	9.65	0.515	1.26

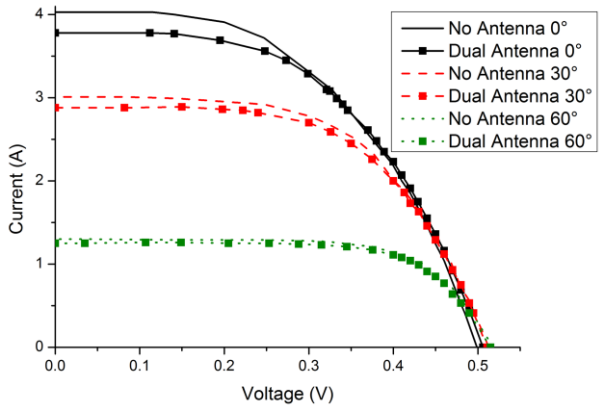

Fig. 6. Measured solar output at various incident angles

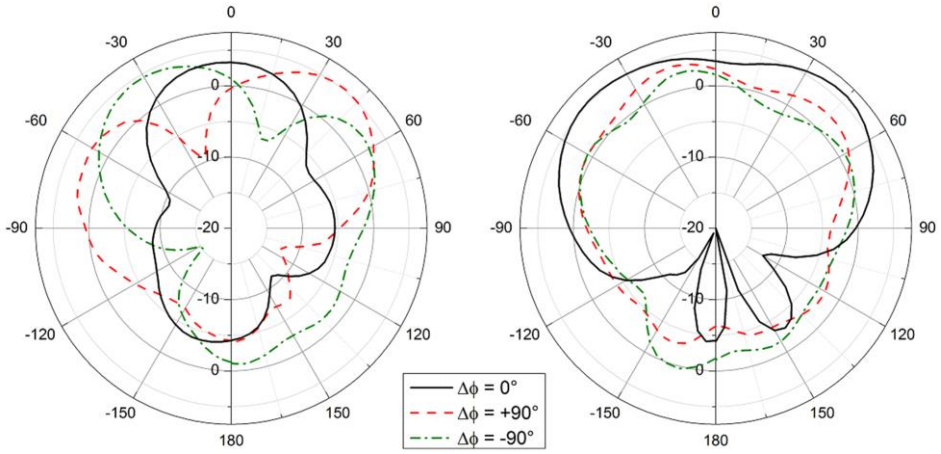

Fig. 7. Measured beam switching for array phase offset (Δφ) in X-Z plane (left) and Y-Z plane (right)

Considering the I_{sc} values, for θ = 0º, 5.30% of the solar cell area is shaded yet measured results show a 5.5% degradation in the solar output. For θ = 30º, 6.18% shading occurs yet the measurement shows 4.3% degradation. For θ = 60º, the 9.65% shadow corresponds to a 3.1% reduction in the measured output. The results indicate that the reduction of the effective solar cell area due to oblique angling of the light source is more significant than antenna shadowing. The average power yielded to a battery would depend on the solar climate conditions in a given location.

Without antennas, the area of the exposed silicon was considered and the reduction in the effective aperture area due to oblique light incident angles was calculated. The maximum power point (MPP) for each angle was extracted from measured data. Analysis shows that for a 30º angle, the area of exposed silicon to the light source is reduced by 13.4% and the measured MPP drops by 12.3% compared with the 0º angle. Similarly, for a 60º incident angle, the exposed area is 50% of the silicon area with a 55% drop in MPP.

V. Beam Switching

Blind zones due to the relatively narrow 60.2º beamwidth of the antenna array in the X-Z plane can be counteracted by implementing beam switching. Measurements were carried out with phase shifts Δφ = 0º, +90º and -90º between the feeds to the two antennas.

The Δφ = 0º phase shift was obtained using a microstrip power splitter with quarter wave transformers to return the microstrip lines to 50 Ω. A single-box branch line coupler was used for the Δφ = +90º case and a rat race coupler was used to produce the Δφ = -90º phase shift.

With a Δφ = 0º phase shift, the main lobe has a peak broadside gain of 3.33 dBi. The Δφ = +90º phase shift produces a 5.24 dBi peak gain at θ = +39º. The Δφ = -90º phase shift provides a 4.52 dBi gain main lobe at θ = -31º. Measured beam switching patterns are shown in Fig. 7.

VI. Conclusions

The first integration of a low profile dual inverted-F antenna array on the bus bars of a photovoltaic solar cell is reported. The 5.3% coverage of the solar cell area is a considerable improvement on previous integrated solar patch antennas which covered 13% of the cell.

Shadow casting tests show that the antenna shadow has less impact than oblique angles of incidence. Oriented directly at a 1450 Lux light source, the antenna reduction of solar power output is limited to 5.5%.

The dual antenna array covers more of the solar cell area than a single element IFA but the gain has a 3 dB improvement with a slightly larger beamwidth in the Y-Z plane and the ability to cover a larger angular sector in X-Z plane by implementing beam switching. It also compares favorably to patch antenna integrations by providing wider bandwidth and higher gain. Beam switching offers flexible pattern configurations for different mounting angles.

References

[1] A. Georgiadis, A. Collado, S. Kim, H. Lee and M.M. Tentzeris, "UHF Solar Powered Active Oscillator Antenna on Low Cost Flexible Substrate for Wireless Identification Applications" *IEEE Intl MTT-S*, 2012.

[2] S.V. Shynu, M.J. Roo~Ons, M.J. Ammann, S.J. McCormack, B. Norton, "Dual Band a-Si:H Solar-Slot Antenna for 2.4/5.2GHz WLAN Applications" In Proc. 3rd Eur. Conf. on Antennas & Propag., 2009, pp. 408-410.

[3] J. Huang, M. Zawadzki, "Antennas Integrated with Solar Arrays for Space Vehicle Applications" In Proc. 5th Intl Symp on Antennas Propag. & EM Theory, 2000, pp. 86-89.

[4] N. Henze, M. Weitz, P. Hofmann, C. Bendel, J. Kirchhof, H. Fruchting, "Investigation of Planar Antennas with Photovoltaic Solar Cells for Mobile Communications" In Proc. IEEE International Symposium on Personal Indoor and Mobile Radio Communications, 2004, pp. 622-626.

[5] O. Yurduseven, D. Smith, "A Solar Cell Stacked Multi-Slot Quad-Band PIFA for GSM, WLAN and WiMAX Networks" *IEEE Microwave & Wireless Component Letters*, vol. 23, no. 6, June, pp. 285-287, 2013.

[6] S.V. Shynu, M.J. Roo~Ons, P. McEvoy, M.J. Ammann, S.J. McCormack, B. Norton, "Integration of Microstrip Patch Antenna with Polycrystalline Silicon Solar Cell" *IEEE Trans Antennas and Propag*, vol. 57, no. 12, December, pp. 3969-3972, 2009.

[7] S.V. Shynu, M.J. Ammann, S.J. McCormack, B. Norton, "Emitter-wrap-through photovoltaic dipole antenna with solar concentrator" *Electron. Lett.* vol. 45, no. 5, pp. 241-242, 2009.

[8] O. Yurduseven, D. Smith, N. Pearsall, I. Forbes, F. Bobor-Oyibo, B. Norton, "A Solar Parabolic Reflector Antenna Design for Digital Satellite Communication Systems" *CSNDSP*, 2012.

[9] O. O'Conchubhair, P. McEvoy, M.J. Ammann, and G. Ruvio, "Integration of Inverted-F Antenna with Solar Cell Substitute" In Proc. LAPC – Loughborough Antennas & Propagation Conference, 2012, pp. 1-4.

[10] Solland Solar Cell BV, *DSO 00306*, Dec, 2006.